

# **Thermo-metallurgical model for hot rolled strip**

G. Gomez, J. Schicht, M.A. Vicente Alvarez, F. Balzarotti, T. Perez  
R&D Tenaris Siderca, Campana, Buenos Aires, Argentina

M. Goldschmit  
IMATEC, Engineering School, Universidad de Buenos Aires, Argentina

J. Moriconi  
TerniumSiderar, San Nicolas, Buenos Aires, Argentina

Keywords: Thermo-metallurgical model, Hot rolling product, Cooling table, Mechanical properties

## **Abstract**

A coupled thermo-metallurgical model was developed to predict the mechanical properties of hot rolled steel strips all along the coil length. The thermal finite element (FE) model solves the heat diffusion equation considering the transformation enthalpy produced by the austenite decomposition. In the run out table, the thermal model evaluates the temperature evolution considering the heat extraction due to the water sprays. After coiling, the model solves the thermal evolution in the cylindrical geometry. The metallurgical model calculates the kinetic of austenite decomposition and evaluates the transformation enthalpy. It also predicts the grain size, pearlite lamellar spacing and precipitation of elements in solid solution.

The predictions of the coupled model were compared with temperature measurements at the end of the run out table (coiling temperature) for C-Mn and microalloyed steels with excellent agreement. Moreover the predicted yield strength and ultimate tensile strength had a good agreement with measurements performed on more than 130 plant processed coils.

## **1. Introduction**

The steel chemical composition and the thermo mechanical treatment applied during hot rolling, cooling and coiling determine the final microstructure of the hot rolled strip, and in turn their mechanical properties. Usually the mechanical properties are measured at the end of the coil and checked to fulfill the product requirements. However, the processing conditions are not the same along the whole strip length, which can give rise to different mechanical properties along the coil length. In order to predict possible deviations, it is of paramount importance to have a tool capable to accurately predict the mechanical properties not only at the end but at any point inside the coil. In that direction, Ternium Siderar together with the R&D Center at Tenaris Siderca have carried out a research project to model the thermal and metallurgical evolution of the strip during the hot rolling and coiling processes.

The cooling table model, called Thermet, was based on previously published works on thermal evolution of plates during water jet impingement [1-6], as well as some existing non-coupled [3; 4; 7-11] and coupled [12-14] thermo-metallurgical models.

Thermet consists of a metallurgical model coupled to a thermal finite element model. The metallurgical model calculates the austenite decomposition into ferrite, pearlite and/or bainite. It also evaluates the enthalpy and specific heat of the system needed for the coupling with the thermal model. A more extensive description of the coupled model and validation is described in Ref. [15,16].

In this paper, some improvements to Thermet were incorporated, the austenite grain size after rolling is evaluated through a metallurgical model of the rolling processes [17,18], the thermal evolution of the material during coiling was estimated using a FE model considering the proper boundary conditions of the coil and a module to evaluate the mechanical properties from the microstructural variables was included.

The whole model was tested against thermal measurements and mechanical properties determination on coils processes at TerniumSiderar.

In Section 2 and 3 a brief description of the thermal and metallurgical models are presented. In Section 4 the mechanical properties evaluation module is outlined. In Section 5 the boundary conditions in the particular case of the run-out table at TerniumSiderar are described. In Section 6 the results of the comparison with C-Mn and microalloyed steels are presented. Finally, in Section 7 the main conclusions are summarized.

## 2. Thermal finite element model

For an isotropic material the heat diffusion equation to be solved by the finite element method [19] is

$$\frac{\partial h}{\partial t} - \nabla \cdot (k \nabla T) = 0 \quad (1)$$

where  $h$  is the enthalpy of the solid solution,  $k$  is the thermal conductivity and  $T$  the temperature. For each material point,  $h$  is function of the temperature and the phase distribution.

The first term of the diffusion equation can be dealt as follows

$$\frac{\partial h}{\partial t} = \frac{\partial h}{\partial T} \Big|_{X^\phi} \frac{\partial T}{\partial t} + \frac{\partial h}{\partial X^\phi} \Big|_T \frac{\partial X^\phi}{\partial t} \quad (2)$$

where the derivatives are calculated by the metallurgical model:

$$\frac{\partial h}{\partial T} \Big|_{X^\phi} = C_p = -T \left( \frac{\partial^2 G}{\partial T^2} \right)_P \quad (3)$$

where  $C_p$  is the specific heat,  $G$  is the free energy Gibbs and  $P$  is the pressure.

The derivation of eq. (3) is made on a fixed temperature interval, using the present step temperature and the previous step microstructure. The release heat during the reaction per unit time ( $L$ ) is

$$\left. \frac{\partial h}{\partial X^\phi} \right|_T \frac{\partial X^\phi}{\partial t} = \frac{\partial h}{\partial t} - C_p \frac{\partial T}{\partial t} = L \quad (4)$$

Between two time steps ( $t, t+\Delta t$ ),  $L$  is calculated with the following expressions

$$L = \frac{\left( {}^{t+\Delta t}h - {}^t h \right) \Big|_{{}^{t+\Delta t}T}}{\Delta t} \quad ; \quad h = G - T \left( \frac{\partial G}{\partial T} \right)_p \quad (5)$$

The derivation of eq. (5) is made on a fixed temperature interval, using the present step temperature. The nonlinearity due to the dependency of the temperature with the properties is solved using a Line Search scheme [20]. The transient heat transfer equation is solved using an implicit Euler Backward time integration method [19].

### 3. Metallurgical model for phase transformation and microstructural evolution

The metallurgical model for phase transformation from the austenitic range during cooling was described in detail elsewhere [16,21]. For simplicity the austenite decomposition was divided in two stages: i) the transformation start, which includes the first 1% of the reaction (in volume fraction), and ii) the reaction progress, which includes the rest of the transformation. For the range of steel chemistries and processing conditions considered in this work, the transformation start comprises the proeutectoid ferrite nucleation and its early growth. The transformation progress includes the remaining ferritic reaction, as well as the other possible reactions: formation of pearlite and/or bainite.

The start of the proeutectoid ferrite reaction was evaluated using classical nucleation and growth theories in combination with the extended volume formalism [22]. The coherent pillbox model for ferrite nucleation at austenite grain boundaries [23] together with the carbon diffusion coefficient of Agren [24] and the interfacial energies reported by Tanaka *et al.* [25] were used to evaluate the nucleation rate. The number of nucleation sites per unit volume was taken proportional to the austenite grain boundary area per unit volume:  $N = N_0 / d_\gamma$  where  $d_\gamma$  is the austenitic grain size and  $N_0$  is a parameter to be empirically adjusted. The physical model for nucleation and early growth of ferrite has only that empirical parameter. For all the steels studied the same  $N_0$  value was used, which was fitted by comparison between model predictions and experimental results for C-Mn steels [21]. Since no intragranular nucleated ferrite was experimentally observed in the ranges of steel chemistries and cooling rates studied, this type of nucleation was not considered in the model.

Within the paraequilibrium approach, the growth of the ferrite nucleus was considered to be controlled by diffusion of carbon in austenite, and was evaluated using:

$$\frac{dr}{dt} = F(\Omega) \frac{D_C^\gamma}{r} \quad ; \quad \Omega = \frac{c^{\gamma\alpha} - c^\gamma}{c^{\gamma\alpha} - c^{\alpha\gamma}} \quad (6)$$

where  $r$  is the radius of the ferrite grain;  $c^{\gamma\alpha}$ ,  $c^{\alpha\gamma}$  and  $c^\gamma$  are the carbon concentrations in austenite in equilibrium with ferrite, in ferrite in equilibrium with austenite, and in austenite far from the growing nucleus, respectively.  $D_C^\gamma$  is the diffusion coefficient of C in austenite. The function  $F$

depends on the super-saturation ratio  $\Omega$ , and was evaluated using the stationary-interface approximation for  $|\Omega| < 0.7$  and the linearized-gradient approximation for  $|\Omega| \geq 0.7$  [26].

The progress of the proeutectoid ferrite, pearlite and bainite reactions was described using Avrami type equations:

$$\chi^\phi / \chi_{eq} = 1 - \exp[-\Psi \cdot t^n] \quad (7)$$

where  $\chi^\phi$  is the volume fraction occupied by phase  $\phi$  at time  $t$  ( $\phi$ : ferrite, pearlite or bainite), and  $\chi_{eq}$  is the thermodynamic equilibrium fraction for proeutectoid ferrite, or the maximum available volume fraction in the case of pearlite and bainite. The following functional form of  $\Psi$  was adopted:

$$\Psi = \frac{A(T - T_0)^p \exp(-Q/RT)}{F(d_\gamma, \text{chemistry})} \quad ; \quad F(d_\gamma, \text{chemistry}) = \exp(B_0 + \sum B_j C_j) / d_\gamma^m \quad (8)$$

where  $d_\gamma$  is the previous austenitic grain size,  $T_0$  is the start temperature for each reaction, and  $C_j$  is the weight percent concentration of the element  $j$  in solid solution in austenite ( $j$ : C, Mn, Si, Nb, V),  $Q$  is an activation energy. The starting temperature for the proeutectoid ferrite, pearlite and bainite reaction were evaluated as indicated in ref [16]. The empirical parameters  $A$ ,  $Q$ ,  $B_0$ ,  $B_j$  and that appear in eq. (8) were fitted for each possible reaction (ferrite, pearlite or bainite) using data obtained from bibliography and from dilatometric tests performed on plain carbon and microalloyed steels [16,21].

The ferrite grain size is given by the following expression:

$$d = A \cdot \exp\left(-\frac{TAe3 - T_s^F}{b}\right) \cdot d_\gamma^c \cdot \chi_F^m \quad (9)$$

where  $T_s^F$  is the start temperature for the formation of ferrite, and  $\chi_F$  is the fraction of ferrite after transformation. The parameters  $A$ ,  $b$ ,  $c$  and  $m$  were fitted with laboratory simulations performed on different steels [21].

The interlamellar spacing is calculated using the expression proposed by Badheshia [27]:

$$\lambda = V_p \cdot \frac{TAe1}{L_p \cdot (TAe1 - T_s^P)} \quad (10)$$

where  $V_p$  is the volume of pearlite,  $L_p$  is a typical length and  $T_s^P$  is the starting temperature for pearlite reaction.

Coarsening of both ferrite grain size and lamina spacing is included in the calculation.

The dislocation density after transformation is estimated by an empirical relation given by:

$$\rho = \rho_0 \cdot \exp(Q_d / RT_m) \quad (11)$$

where  $T_m$  is the average between the starting and finishing temperature for the ferrite reaction,  $\rho_0$  and  $Q_d$  are fitting parameters [21].

Several types of precipitates are considered to form in ferrite: TiC, AlN, Nb(C,N), NbV(C,N), and V(C,N). Which precipitate forms depends on the amount of the elements in solid

solution. In particular, it is assumed that Ti is tight to N during casting, so the effective amount of both Ti and N after transformation can be considerable reduced. Each time step, the amount of elements in solid solution is updated, and new conditions for the precipitation reactions occur.

The calculation of precipitation kinetic is based on classical nucleation and growth kinetic. The basic equations can be found elsewhere [28]. It is assumed that nucleation can occur either on dislocations or at grain boundaries, and the rate of nucleation is controlled by the chemical energy for the reaction. The growth kinetic is controlled by the diffusion of the interstitial atoms (bulk and dislocation assisted) and spherical nuclei are assumed. Coarsening of precipitates is also considered.

#### 4. Prediction of mechanical properties after transformation

The  $YS$  and  $UTS$  of the material are evaluated as a function of the  $YS$  and  $UTS$  of each phase following Pickering [30]:

$$YS = \chi_F^{YS} YS_F + \chi_P^{YS} YS_P + \chi_B^{YS} YS_B + YS_{\rho+pre} \quad (12)$$

$$UTS = \chi_F^{UTS} UTS_F + \chi_P^{UTS} UTS_P + \chi_B^{UTS} UTS_B + UTS_{\rho+pre} \quad (13)$$

where  $YS_i$  and  $UTS_i$  are the yield strength and ultimate tensile strength of phase  $i$ ,  $\chi_i^{YS}$  and  $\chi_i^{UTS}$  are the weights of phase  $i$  to  $YS$  and  $UTS$ , respectively. For the  $UTS$ ,  $\chi_i$  is simply the fraction of phase  $i$  at the end of transformation. For the  $YS$ ,  $\chi_i$  is a function of the fraction of ferrite and pearlite and it account for the fact that the  $YS$  of a dual phase material is more close to the  $YS$  of the softer phase than that predicted by lineal addition.  $YS_{\rho+pre}$  and  $UTS_{\rho+pre}$  are the contribution due to dislocation and precipitation hardening.

For both ferrite and pearlite the classical expressions for  $YS$  are used [29]:

$$YS_i = YS_0 + \sum_{sust} C_x [X] + \frac{YS_d}{\sqrt{d}} \quad (14)$$

where  $YS_0$  is the friction term, the second term corresponds to the contribution of the elements in solid solution and the third term is the Hall-Petch equation which relates the  $YS$  with the characteristic length for dislocation motion of the phase, for ferrite the grain size and for pearlite the interlamellar spacing. Similar equations are used to evaluate the  $UTS$  of the phases. For bainite the equation proposed by Pickering are used [30].

The contributions to Eqs.(12) and (13) of the dislocations and precipitates formed in the ferrite phase are summed in a quadratic way. The dislocation density term was assumed proportional to the dislocation density, Eq. (11). The contribution of the precipitates is calculated

using the well known equation:  $\frac{6\sigma f_v}{\pi r_p}$ , where  $\sigma$  is a surface energy,  $f_v$  and  $r_p$  are the volume fraction and radius of the precipitates, respectively [29]. When precipitation is negligible, the contribution of the dislocations to the mechanical properties is disregarded, since recovery occurs

## 5. Application of the thermo- metallurgical model to the TerniumSiderar hot rolled strip

After hot rolling the strip is cooled in the runout table and then coiled. A diagram of TerniumSiderar cooling table is shown in Figure 1.

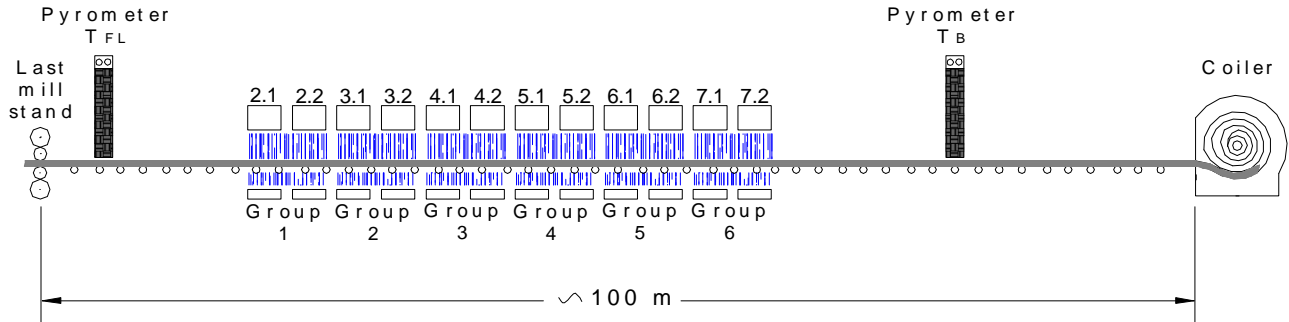


Figure 1 – TerniumSiderar cooling table scheme.

In both the upper and the under side of the cooling table, the strip is cooled by several groups of water jets that impinge on it. To ascertain the strip temperature along the runout table, pyrometers are placed at the beginning and at the end of the cooling table.

The cooling of the strip in the runout table is modeled using three different heat transfer coefficients that take into account the different cooling regimes: the first one is the dry zone between the last roll and the first water spray; the second one is the wet zones where the water jets impinge on the strip surface. In this stage the heat transfer coefficient is modeled using a Hodgson formulation [31, 32] that depends on the strip temperature and speed, and on the water flux rate. The third regime is the humid zones where residual water creates a stable boiling film. In this stage a coefficient presented by Chang [33] that takes into account steam physical properties and the temperature surface, is used to model the heat transfer.

The fitting of the heat transfer coefficient parameters was done by comparing the temperature measured by the pyrometer before coiling and the predictions of the model using as input the actual rolling finishing temperature and the cooling process parameters. A more detailed description of the fitting procedure is presented in Reference [16].

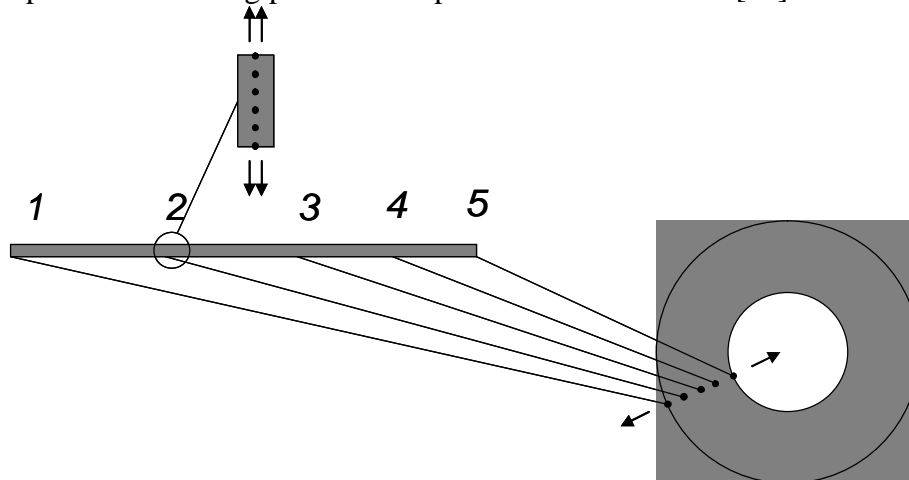


Figure 2: Mapping of the sections in the cooling table and the coil.

After the cooling table, the strip is coiled. To model this part of the process two convection coefficients are used one for the inner and the other for the outer turns of the coil. The coefficient used for the inner surface is lower than that for the outer surface and were fitted based on temperature measurements performed on plant coils.

The problem is solved in two steps, first the model is run for all the sections of the strip in the cooling table, then the nodes are mapped to the coil geometry and the thermo-metallurgical evolution of a radial section of the coil is calculated. Figure 2 presents a scheme of how the different sections of the strip are mapped from the cooling table to the coil. In the runout table the heat transfer in the rolling direction can be neglected compared to the heat extraction in the thickness direction, therefore the thermo-metallurgical evolution of each section can be treated separately and solving the entire strip is not more than solving  $n$  independent sections. When the strip is in the coil geometry this approximation cannot be applied since the heat flux in the radial direction is relevant, therefore the problem has to be solved at once. When mapping, the temperature and metallurgical variables (fraction of phases) must be appropriately transferred. As for each node of the coil there are several corresponding nodes in the cooling table, we decided to take the values at the node placed at the middle of the thickness.

## 6. Results

Thermet was run for 137 coils of different chemical composition (including C-Mn and microalloyed steels) that were processed under different conditions. In Table 1 the ranges of chemical compositions studied are outlined.

**Table 1: Ranges of chemical composition studied.**

C	Mn	Si	Al	N2	Nb	Ti	V
0.025-0.16	0.16-1.3	<0.17	0.02-0.06	20-80ppm	<0.05	<0.03	<0.08

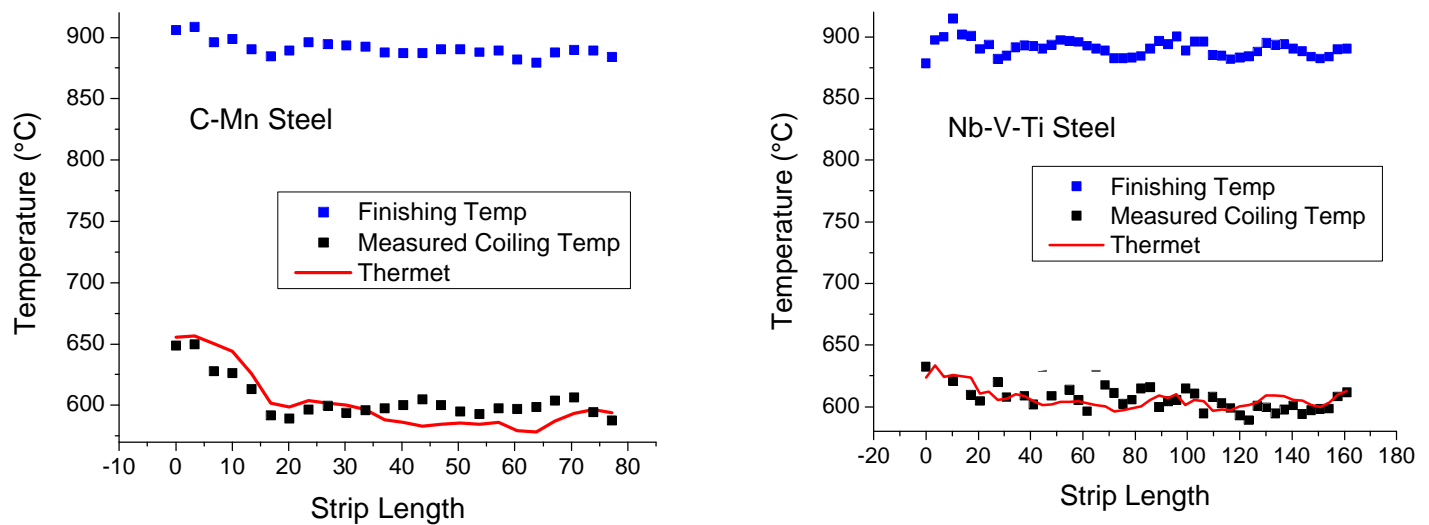


Figure 3: Comparison between the measured coiling temperature and the predicted by the model for a C-Mn steel. The final rolling temperature is included.

The austenitic grain size and the amount of elements in solid solution prior cooling were predicted by a metallurgical program that models the real industrial hot rolling from the overheating furnace to the runout table. The model takes into account the temperature reached in the overheating furnace, the steel chemical composition and the hot rolling sequence (amount of deformation, deformation rate, temperature in each pass and strip speed) [17,18].

Figure 3 shows a comparison between the predicted coiling temperature and the measured one for a C-Mn (left) and for a microalloyed (Nb-V-Ti) steel (right) as a function of the strip length. The hot rolling finishing temperatures are also included. The agreement between numerical results and measurements is good in both cases. Small variations of the coiling temperature along the strip length are observed due to changes of the processing conditions. The model is capable to reproduce these variations. It is worth to mention that the latent heat of austenite decomposition is comparable with the heat extracted by the water jets, so this result is not only indicating that the thermal model is accurate but that the metallurgical model is also reliable. As we will show next, the transformation kinetics of a C-Mn and that of a microalloyed steels are quite different.

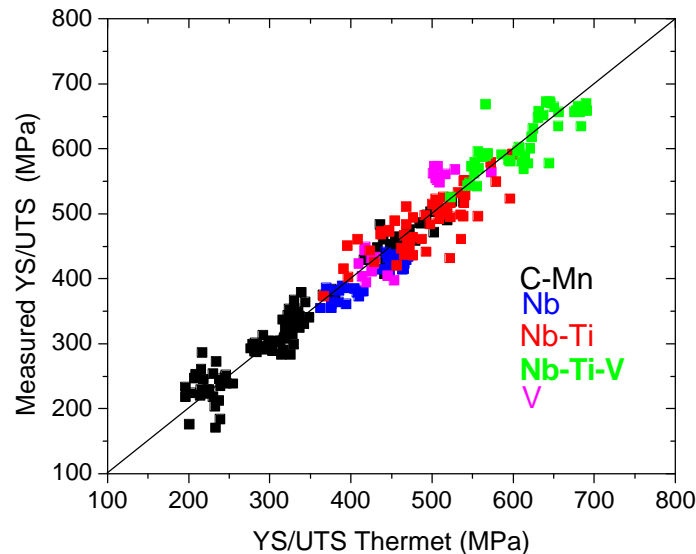


Figure 4: Comparison between Thermet and measured YS and UTS values for the last turn of the coil.

In Figure 4 the mechanical properties (YS and UTS) predicted by Thermet are compared to those measured at the end of the strip (corresponding to the outer turn of the coil) for all the coils. The agreement is good for all the range studied. The C-Mn coils have YS values from 200MPa (lowest C and Mn contents) to 400MPa (Mn around 1wt% with additions of Si). Four types of microalloyed steels were studied, Nb, Nb-Ti, Nb-Ti-V and V steels. The Nb, Nb-Ti and V families have YS values from 400 to 500MPa, finally, the Nb-Ti-V family is the hardest one.

Additionally, the Thermet model gives also as output the mechanical properties and all the metallurgical variables inside the coil. An analysis on how the different phases contribute to the total strength of the material can be straightforwardly done. In the following examples, part of this analysis is presented. Two cases were selected, a C-Mn and a Nb-Ti microalloyed steels. The chemical composition of these materials is outlined in Table 2.

**Table 2: Chemical composition of the case study steels**

Steel	C	Mn	Si	Al	N2	Nb	Ti
C-Mn	0.16	0.76	0.11	0.048	0.0035	-	-
Nb-Ti	0.075	1.3	0.16	0.027	0.0045	0.048	0.018

## C-Mn steel

This material was processed in plant with a coiling temperature in the range 600-660°C. Their mechanical properties (YS and UTS) were measured at the outer turn of the coil and also at the middle of the strip length. Thermet was run following the industrial processing conditions; in Figures 5 to 8 the main results are depicted.

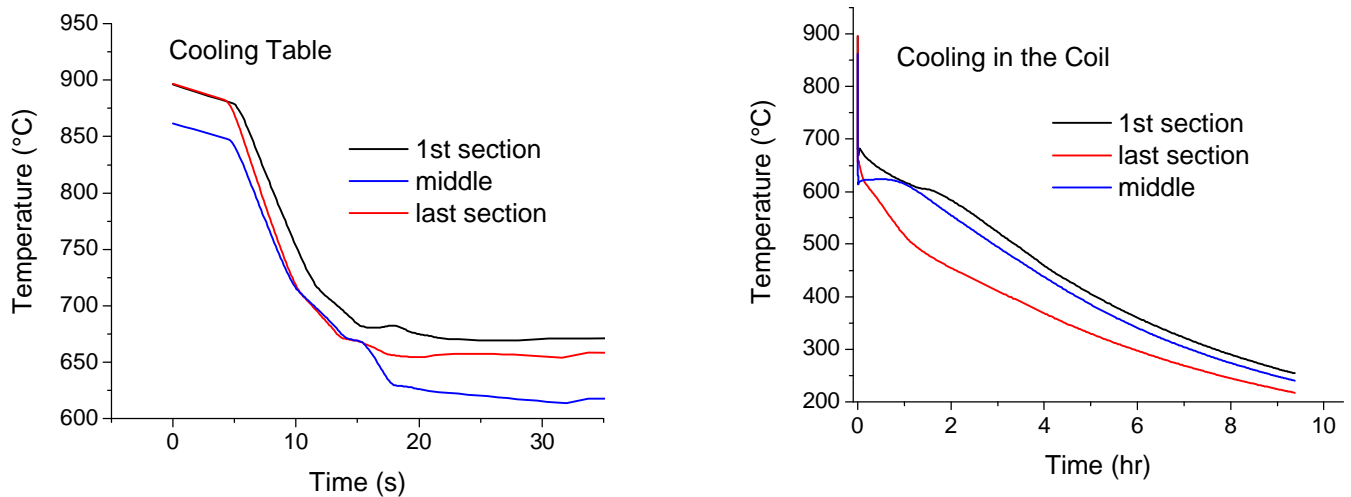


Figure 5: Temperature evolution of a C-Mn steel in the run out table (left) and in the coil (right) for three sections.

The evolution of temperature for three sections of the strip (first, last and middle) is presented in Figure 5. In the left, the first 30 seconds are plotted in detail. This period corresponds to the strip passing through the cooling table. Three regions can be clearly observed, during the first 5 seconds the material cools slowly due to air cooling, then an abrupt fall of the temperature occurs due to water cooling, finally the temperature is stabilized in the humid zone. Each section of the coil finishes with a different temperature before coiling. In the right part of the figure, the evolution of temperature of these sections is plotted. The first section (black line) corresponds to the inner turn of the coil and cools slowly (a low convective coefficient was used for this surface of the coil). At the middle of the coil (blue line) the material cools slowly too, because the heat flux is controlled by conduction in the radial direction. Finally, the outer surface (red line) has the highest cooling rate due to a higher heat extraction.

The kinetic of austenite decomposition is plotted in Figure 6. After 35 seconds the transformation into ferrite and pearlite is complete, no bainite is predicted. The final fraction of the phases is mainly controlled by the carbon content and the kinetic is similar for the two sections analyzed. The middle section has a lower temperature in the run out table (see Figure 5) and that is why the pearlite reaction starts earlier compared to the first section of the strip.

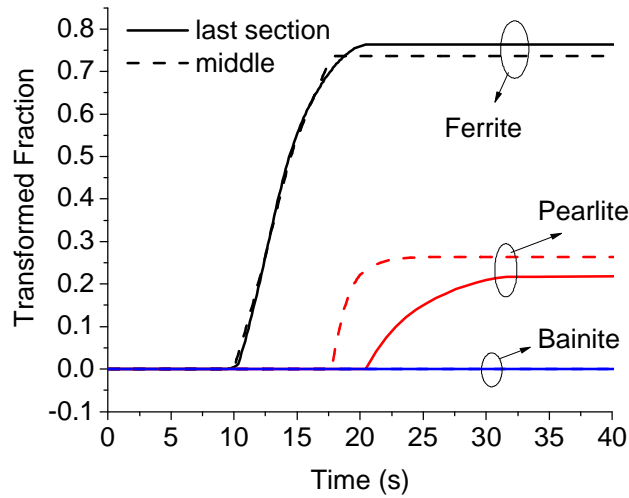


Figure 6: Phase transformation kinetic for the same material of Fig5.

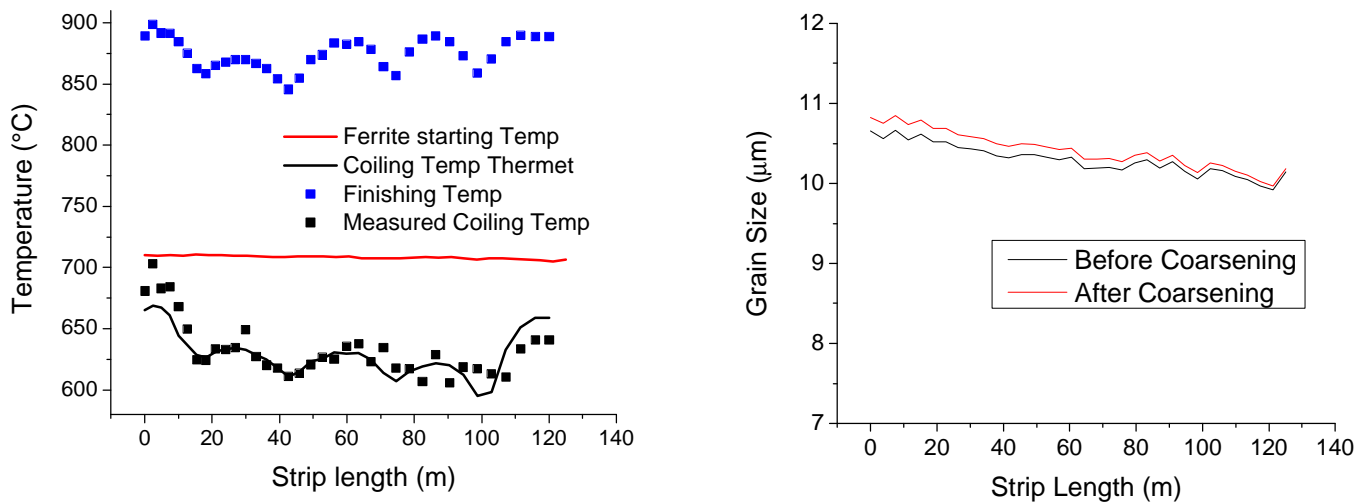


Figure 7: Finishing, coiling and starting transformation temperatures (left), predicted grain size before and after coarsening (right) for the C-Mn steel.

The predicted coiling temperature has a good agreement with the measured one (black line in the left of Figure 7). The model is capable to reproduce well the characteristic bumps in the temperature caused by the skid marks in the reheating furnace. These cold marks survive the hot rolling process, are visible in the finishing temperature (blue line) and are inherited by the coiling temperature. In the Figure the starting temperature for ferrite formation is plotted in red. This temperature is almost constant along the whole length and is around 700°C. This value depends mainly on the cooling rate and steel chemistry, specially the C content, being independent of the finishing temperature. This temperature determines the ferrite grain size at the end of transformation (see Eq.(9)) which is shown in black in the right side of the Figure. In the same figure the grain size after coiling is shown in red. The predicted values are in well

accordance with observed grain sizes for this type of steels ( $\sim 10\mu\text{m}$ ). Coarsening is almost negligible, what is consistent with the asymptotic kinetic of this mechanisms for large grains.

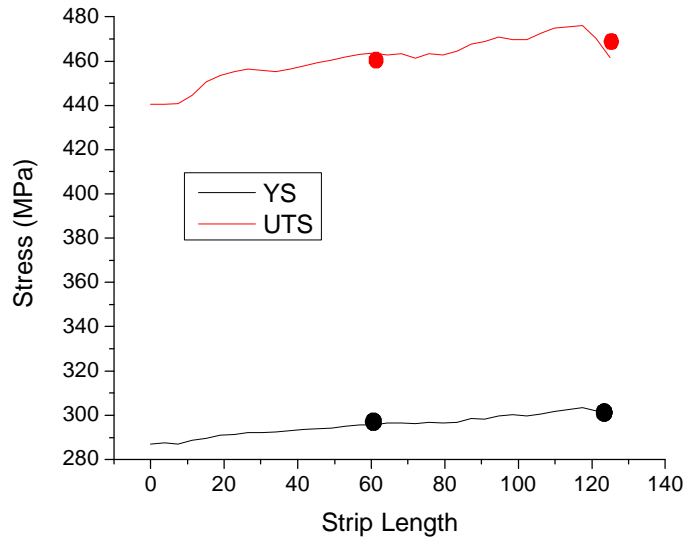


Figure 8: Comparison between the prediction of the model and the measured mechanical properties (at the end and at the middle of the strip length) for the C-Mn steel.

Figure 8 shows a comparison between the predicted YS and UTS values and measurements performed at the end and at the middle of the coil. The agreement is good. The model predicts lower properties at the first sections of the strip (inner surface of the coil). This is due to the differences in the grain size (right of Figure 7) together with differences in the final fractions of ferrite and pearlite.

### Nb-Ti steel

Compared to the C-Mn steel, the Nb-Ti material has a lower C, higher Mn and important additions of Nb and Ti (Table 2). These changes of the steel chemistry will have important effects on the transformation kinetic. The Thermo model was run for the plant processing condition and the results are shown in Figure 9 and 10.

On the left side of Figure 9 the predicted coiling temperature is compared to the measured one. The agreement is good, there is a light overestimation for the strip sections between 50 and 100m. For this coil the skid marks are not observed. The ferrite starting temperature is shown in red. This temperature is almost similar to the coiling temperature, and is around  $650^{\circ}\text{C}$ . It is clear that the important delay on the ferrite transformation due to the Nb addition is responsible for this behavior (Ti in solution is almost negligible since it was tight to N during casting). In contrast to the C-Mn steel, the initiation of the ferrite transformation depends to some extent on the coiling temperature, what is relevant since this implies possible influences of the coiling temperature on the final grain size.

In the right part of Figure 9 the ferrite grain size at the end of transformation (black) and after coarsening (red) are presented. The grain size at the end of transformation is almost constant as a function of the coil length and around  $4\mu\text{m}$ , much smaller than that predicted for

the C-Mn steel. Important coarsening is predicted for the whole coil, the grain size increases to 5.5 $\mu\text{m}$  for the outer surface of the coil and up to 7.5 $\mu\text{m}$  for the inner part of the coil.

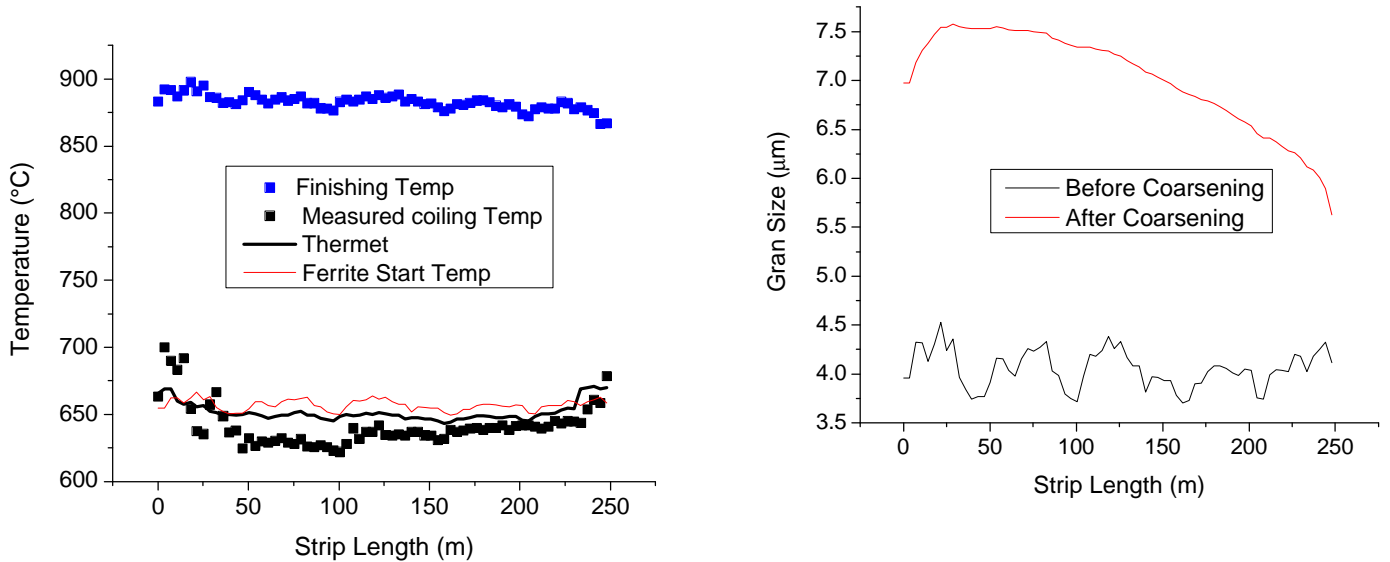


Figure 9: Finishing, coiling and starting transformation temperatures (left), predicted grain size before and after coarsening (right) for the Nb-Ti steel.

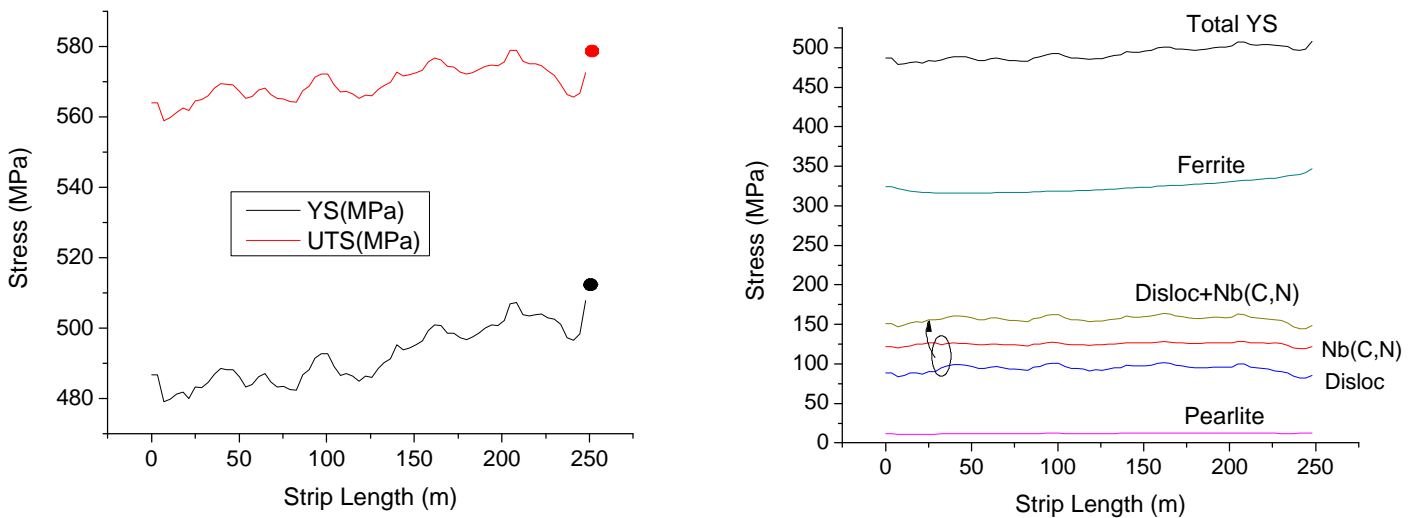


Figure 10: Left: Comparison between the prediction of the model and the measured mechanical properties (at the end of the strip length) for the Nb-Ti steel. Right: Contribution of the different mechanisms to the YS.

Figure 10 shows the predicted mechanical properties compared to those measured at the end of the coil. Again the agreement is good. In the right part of the figure a decomposition of the total YS into the contributions of ferrite, pearlite, dislocations and precipitates is shown. The most important contribution comes from ferrite with a fraction of ~90%. Note that despite the important differences in the final grain size (Figure 9) the ferrite strength shows variation of only 30MPa. The second contributor is the dislocations and precipitates term, with ~150MPa. This

term is formed by the quadratic addition of the contribution of Nb(C,N) precipitates (around 120MPa) and dislocation (80MPa). Finally, due to its low fraction the contribution of pearlite to the final YS is negligible.

## 7. Conclusions

A coupled thermo metallurgical model was developed for TerniumSiderar cooling table and coiler.

The model is capable to predict with a good accuracy the coiling temperature and the mechanical properties of a wide range of steel chemistries. It has as output, the thermal evolution in the run out table and coiler, the kinetic of austenite decomposition into ferrite, pearlite and bainite, the metallurgical variables that determine the strength of each phase and the final mechanical properties.

The coiling temperature predictions were validated with measurements performed in plant for more than 130 C-Mn and microalloyed steel coils. The mechanical properties predictions were validated with measurements performed at the outer surface of the coils and in few cases at the middle of the coil length.

The thermo-metallurgical model can be used as a design tool, or can be run online to detect deviation of mechanical properties inside the coil.

## Acknowledgments

We want to acknowledge Tenaris Siderca and Ternium Siderar for the financial support.

## References

- [1] N. Hatta, Y. Tanaka, H. Takuda and J. Kokado, *ISIJ International*, 1989, no 8: 673-679.
- [2] N. Hatta and H. Osakabe, *ISIJ International*, 11 (1989), 919-925.
- [3] M. Raudensky, L. Bending, J. Horsky, *Steel Research*, 1 (1994), 29-35.
- [4] V.H. Hernandez, I.V. Samarasekera, J.K. Brimacombe, "Heat transfer model of runout table cooling: a fundamental approach" (Paper presented at the 36th Mechanical Working and Steel Processing Conference Proceedings, 1995), 345-356.
- [5] J. Fry, H. Morgan, W. Morris, J. Medwell, *Ironmaking and Steelmaking*, 1 (1997), 1:47-52.
- [6] H. Robidou, H. Auracher, P. Gardin, M. Lebouché, *Experimental Thermal and Fluid Science*, 26 (2002), 123-129.
- [7] J.E. Evans, I. D. Roebuck, H.R. Watkins, *Iron and Steel engineer*, 1 (1993), 50-55.
- [8] J. Filipovic, R. Viskanta, F.P. Incropera, "Cooling of a moving steel strip by an array of round jets," (paper presented at 35th Mechanical Working and Steel Processing Conference Proceedings, 1994), 317-327.
- [9] T. Kato, Y. Hayasi, T. Kuraishi, S. Ayano, T. Kashimazaki, "New temperature control system of hot strip mill run out table," (Paper presented at 36th Mechanical Working and Steel Processing Conference Proceedings, 1994), 311-316.
- [10] M.M. Prieto, L.S. Ruiz and J. Menéndez, *Ironmaking and steelmaking*, 6 (2001), 474-480.
- [11] S.D. Cox, S.J. Hardy, D.J. Parker, *Ironmaking and Steelmaking*, 5 (2001), 363-372.

- [12] A. Kumar, C. McCulloch, E.B. Hawbolt, I.V. Samarasekera, *Materials, Science and Technology*, 7 (1991), 360-367.
- [13] A. Prasad, S. Jha, N. Mishra, *Steel Research*, 10 (1995), 416-423.
- [14] A. Prasad, S. Jha, N. Mishra, *Steel Research*, 10 (1995), 416-423.
- [15] J. Schicht, "Modelo Termo-Metalúrgico aplicado al enfriamiento de aceros" (Mechanical degree Thesis, Buenos Aires University, 2004).
- [16] Gomez, G. Schicht, J. Perez, T. Goldschmit, M. Vigliocco, A., "Thermo-Metallurgical Model of the Cooling Table for a Flat Product Hot Rolling Mill", MS&T2006, pp443-454.
- [17] G. Gomez, T. Pérez, "Modelling the microstructural evolution during hot rolling", *Latin American Applied Research*, 32 (3), 253-256, 2002.
- [18] G. Gomez, T. Pérez and J. Moriconi, "Modelling the Microstructural Evolution during Hot Strip Rolling" (Paper presented at the 44th Mechanical Working and Steel Processing Conference Proceedings, 2002), 1093-1103.
- [19] O.C. Zienkiewicz and R.L. Taylor, *The finite element method* (Vol 1, Ed. Butterworth Heinemann, 2000).
- [20] H. Matthies and G. Strang, *International Journal for Numerical Methods in Engineering*, 14 (1979), 1613-1626.
- [21] G.R. Gomez, M. Bühler and T. Perez, "Austenite decomposition in low carbon steels with microalloy additions", (Paper presented at Proceedings of the International Conference on Microalloying for New Steel Processes and Applications, Donostia-San Sebastian, Spain, September 2005), 395.
- [22] J.W. Christian, *Theory of Transformations in Metals and Alloys*, (2nd ed. Part I, Pergamon Press, Oxford, United Kingdom, 1975).
- [23] M. Enomoto and H.I. Aaronson, *Metall. Mater. Trans.*, 17A (1986), 1385.
- [24] J. Ågren: Scripta, *Metallurgica*, 20 (1986), 1507.
- [25] T. Tanaka, H.I. Aaronson and M. Enomoto, *Metall. Mater. Trans.*, 26 (1995), 547.
- [26] H.B. Aaron, D. Faistein and G. Kotler, *Journal of Applied Physics*, 41 (1970), 4404.
- [27] H.K.D.H. Badheshia, R. W. K. Honeycombe, in "Steel microstructure and properties", Elsevier Third Edition 2006.
- [28] D.A. Porter and K. E. Easterling, in "Phase transformation in metals and alloys", Chapman & Hall 1997.
- [29] T. Gladman, in "The Physical Metallurgy of Microalloyed Steels", Institute of Materials 1997.
- [30] F. B. Pickering, in "Hardenability concepts with application to steel", Proceedings October 1977, pp. 179.
- [31] P.D. Hodgson, K.M. Browne, D.C. Collinson, T.T. Pham and R.K. Gibbs, "A Mathematical Model to Simulate the Thermomechanical Processing of Steel," (Paper presented at Proceedings of 3<sup>rd</sup> Int. Seminar of the International Federation for Heat Treatment, 1993), 138.
- [32] P.D. Hodgson, L.O. Hazelden, D.L. Matthews, R.E. Gloss, "The development and application of mathematical models to design thermomechanical processes for long products," (Paper presented at Microalloying conference proceedings, 1995), 341-353.
- [33] Y.Y. NSU and R.W. Graham, "Transport processes in boiling and two phase system," *American Nuclear society*, (1985).